

# The X-ray Structure of Epoxide Hydrolase from *Agrobacterium radiobacter* AD1

AN ENZYME TO DETOXYIFY HARMFUL EPOXIDES\*

(Received for publication, February 4, 1999, and in revised form, March 9, 1999)

Marco Nardini‡, Ivo S. Ridder‡, Henriëtte J. Rozeboom‡, Kor H. Kalk‡, Rick Rink§, Dick B. Janssen§, and Bauke W. Dijkstra‡¶

From the ‡Laboratory of Biophysical Chemistry and BIOSON Research Institute and the §Laboratory of Biochemistry, Department of Chemistry, University of Groningen, Nijenborgh 4, 9747 AG Groningen, The Netherlands

Epoxide hydrolases catalyze the cofactor-independent hydrolysis of reactive and toxic epoxides. They play an essential role in the detoxification of various xenobiotics in higher organisms and in the bacterial degradation of several environmental pollutants. The first x-ray structure of one of these, from *Agrobacterium radiobacter* AD1, has been determined by isomorphous replacement at 2.1-Å resolution. The enzyme shows a two-domain structure with the core having the  $\alpha/\beta$  hydrolase-fold topology. The catalytic residues, Asp<sup>107</sup> and His<sup>275</sup>, are located in a predominantly hydrophobic environment between the two domains. A tunnel connects the back of the active-site cavity with the surface of the enzyme and provides access to the active site for the catalytic water molecule, which in the crystal structure, has been found at hydrogen bond distance to His<sup>275</sup>. Because of a crystallographic contact, the active site has become accessible for the Gln<sup>134</sup> side chain, which occupies a position mimicking a bound substrate. The structure suggests Tyr<sup>152</sup>/Tyr<sup>215</sup> as the residues involved in substrate binding, stabilization of the transition state, and possibly protonation of the epoxide oxygen.

Epoxide hydrolases (EC 3.3.2.3) are a group of functionally related enzymes that catalyze the cofactor-independent hydrolysis of epoxides to their corresponding diols by the addition of a water molecule. Epoxides are very reactive electrophilic compounds frequently found as intermediates in the catabolic pathway of various xenobiotics. For instance they are the carcinogens formed by bioactivation reactions catalyzed by cytochrome P450. Therefore, conversion of epoxides to less toxic, water-soluble compounds is an essential detoxification step in living cells. Consequently, epoxide hydrolases have been found in a wide variety of organisms, including mammals, invertebrates, plants, and bacteria (1).

Until now most research has been focused on mammalian epoxide hydrolases (2, 3), which, together with glutathione S-transferases, are the most important enzymes to convert toxic epoxides to more polar and easily excretable compounds

(4). However, much progress has recently also been made in the characterization of bacterial epoxide hydrolases (5, 6, 7). These enzymes show a significant sequence homology with those of mammalian origin. They can be easily obtained in large amounts, and they exhibit enantioselectivity with various industrially important epoxides, which makes them promising biocatalysts for the large scale preparation of enantiopure epoxides and/or their corresponding vicinal diols (8). In particular, extensive studies have been performed on the epoxide hydrolase from *Agrobacterium radiobacter* AD1, a Gram-negative bacterium that is able to use the environmental pollutant epichlorohydrin as its sole carbon and energy source (5, 6, 8). This epoxide hydrolase is a soluble monomeric globular protein of 35 kDa with a broad substrate range. Epichlorohydrin and epibromohydrin are its best substrates, and the optimum pH range for catalysis is 8.4–9.0. Sequence and secondary structure analysis suggested that this enzyme belongs to the  $\alpha/\beta$  hydrolase-fold family of enzymes (9). Site-specific mutations indicated Asp<sup>107</sup>, His<sup>275</sup>, and Asp<sup>246</sup> as the catalytic triad residues. The proposed catalytic mechanism involves two steps analogous to haloalkane dehalogenase (10). In the first reaction step, an ester bond is formed between enzyme and substrate by attack of the nucleophilic Asp<sup>107</sup> on the primary carbon atom of the substrate; in the second step, this ester bond is hydrolyzed by a water molecule activated by the His<sup>275</sup>/Asp<sup>246</sup> pair. The reaction proceeds via two different transition states, one during the binding and opening of the epoxide ring and the second during the hydrolysis of the ester intermediate. However, several important questions remained unanswered. Until now it has not been possible to identify the residue responsible for the binding and protonation of the epoxide oxygen, nor was the location known of the oxyanion hole that stabilizes the Asp<sup>107</sup> oxyanion during the hydrolysis of the ester intermediate. Structural information may also resolve why an Asp<sup>246</sup> → Ala mutant still retains some residual activity (6).

Here we report the 2.1-Å resolution x-ray structure of the epoxide hydrolase from *A. radiobacter* AD1 (Ephy).<sup>1</sup> It is the first epoxide hydrolase for which the structure has been solved. The result of this work can provide a general better understanding about the structural basis of the reaction mechanism for this class of important ubiquitous enzymes.

## EXPERIMENTAL PROCEDURES

**Crystallization and Heavy Atom Search**—The epoxide hydrolase from *A. radiobacter* AD1 was cloned, overexpressed, and purified as described previously (6). The stock protein solution, containing 5 mM

\* Financial support was obtained from the European Union (Eulipase contract number BI02-CT94–3013). Work at the ELETTRA synchrotron was supported by the European Union, contract number ERBFMGECT950022. The costs of publication of this article were defrayed in part by the payment of page charges. This article must therefore be hereby marked “advertisement” in accordance with 18 U.S.C. Section 1734 solely to indicate this fact.

The atomic coordinates and structure factors (Iehy) have been deposited in the Protein Data Bank, Brookhaven National Laboratory, Upton, NY.

¶ To whom correspondence should be addressed. Fax: 31-50363-4800; E-mail: bauke@chem.rug.nl.

<sup>1</sup> The abbreviations used are: Ephy, epoxide hydrolase from *A. radiobacter* AD1; DhIA, haloalkane dehalogenase from *X. autotrophicus* GJ10; Pgl, triacylglycerol lipase from *P. glumae*; Hpl, human pancreatic lipase; NCS, noncrystallographic symmetry; r.m.s., root mean square.

TABLE I  
Data collection and single isomorphous replacement including anomalous scattering (SIRAS) analysis

Data set	Native ( $\lambda = 1.0$ Å)	Hg <sup>a</sup> ( $\lambda = 1.0$ Å)	Hg <sup>a</sup> ( $\lambda = 1.5418$ Å)
Space group	C2	C2	C2
<i>a</i> =	146.62 Å	147.15 Å	147.05 Å
<i>b</i> =	100.20 Å	100.14 Å	100.33 Å
<i>c</i> =	96.88 Å	97.70 Å	97.32 Å
$\beta$ =	100.68°	100.94°	100.51°
Resolution	2.1 Å	3.5 Å	4.0 Å
Observations	222,880	65,941	59,453
Unique reflections	73,445	15,782	10,514
Completeness (%) overall (final shell)	91.5 (82.0)	93.9 (91.7)	88.3 (91.2)
$R_{\text{merge}}$ (final shell) <sup>b</sup>	0.06 (0.36)	0.13 (0.23)	0.12 (0.25)
Phasing			
Heavy atom sites		22	22
Phasing power (iso/ano) <sup>c</sup>		1.80/1.87	2.01
Figure of merit (iso/ano) <sup>d</sup>		0.35/0.40	0.42
Figure of merit overall		0.47	
$R_{\text{Cullis}}$ <sup>e</sup>		0.49	0.43

<sup>a</sup> The Hg derivative is ethyl mercury phosphate (C<sub>2</sub>H<sub>5</sub>HgO)<sub>3</sub>PO.

<sup>b</sup>  $R_{\text{merge}} = \sum_i \sum_h |I_{hi} - \langle I_h \rangle| / \sum_i \sum_h I_{hi}$ .

<sup>c</sup> Phasing power is r.m.s.  $(|F_H|/E)$ , where  $|F_H|$  is the heavy atom structure factor amplitude, and  $E$  is the radial lack of closure  $(|F_{PH} - F_P| - |F_H|)$ . iso, isomorphous difference; ano, anomalous difference.

<sup>d</sup> Figure of merit for a given reflection  $h$  is  $m = |F_{\text{best}}|/|F_h|$ .

<sup>e</sup>  $R_{\text{Cullis}} = \sum_h ||F_{PH}| \pm |F_P| - F_{H(\text{calc})}| / \sum_h |F_{PH} \pm F_P|$ .

potassium phosphate, 1 mM EDTA, 1 mM  $\beta$ -mercaptoethanol, 0.02% sodium azide, and 10% glycerol (pH 6.8) was concentrated and extensively washed using 10 mM potassium phosphate (pH 7.0) in a Centrifuge-10 ultracentrifugation concentrator with a 10-kDa cut-off (Amicon) to a final protein concentration of 5.5 mg/ml. The extensive washing procedure is essential to remove the glycerol before crystallization. The glycerol induces high polydispersity in the protein sample, as was determined by dynamic light scattering analysis on a DynaPro 801 instrument (Protein Solutions, Charlottesville, VA). Removing the glycerol resulted in a solution containing particles with a 2.7-nm diameter (apparent molecular mass of 33 kDa) and a polydispersity of 15%. Crystallization experiments with the protein in the presence of glycerol gave only very thin needles as a best result. An initial promising crystallization condition was obtained from a Sparse Matrix screening (11). Refinement of this Sparse Matrix condition resulted in the following crystallization protocol: hanging drops (4  $\mu$ l of protein solution and 4  $\mu$ l of precipitant) were equilibrated against a 1-ml reservoir containing 1.6 to 1.8 M KH<sub>2</sub>PO<sub>4</sub>/K<sub>2</sub>HPO<sub>4</sub> (pH 7.0) at room temperature. After 2 weeks, the experiments were allowed to slowly evaporate to a phosphate concentration of about 2.0 M. The slow increase of the phosphate concentration in the drop results in the appearance of crystals with typical sizes of 0.3  $\times$  0.2  $\times$  0.1 mm<sup>3</sup>. They are highly x-ray-sensitive, and therefore, all data collections were performed at cryotemperature (100 K), using 30% glycerol added to the stabilizing mother liquor (1.8 M KH<sub>2</sub>PO<sub>4</sub>/K<sub>2</sub>HPO<sub>4</sub>) as a cryoprotectant.

The crystals diffract up to 2.1-Å resolution using synchrotron radiation, and they belong to space group C2 with unit cell parameters of *a* = 146.62 Å, *b* = 100.20 Å, *c* = 96.88 Å,  $\beta$  = 100.68°. This unit cell gives a  $V_M$  value of 2.57 Å<sup>3</sup>/Da<sup>-1</sup> assuming 4 molecules in the asymmetric unit. The deduced solvent content of the crystals is 52%. Heavy atom derivatives were prepared by soaking the crystals in solutions obtained by dissolving the heavy atom compounds in the standard mother liquor (1.8 M KH<sub>2</sub>PO<sub>4</sub>/K<sub>2</sub>HPO<sub>4</sub>). The search resulted in only one good isomorphous derivative obtained by soaking a crystal of epoxide hydrolase for 2 days in a solution of 2.0 mM ethyl mercury phosphate, (C<sub>2</sub>H<sub>5</sub>HgO)<sub>3</sub>PO.

**Data Collection and Processing**—A 2.1-Å resolution native data set and one of the two ethyl mercury phosphate derivative data sets were collected at the x-ray diffraction beamline of the ELETTRA synchrotron in Trieste (Italy), equipped with a 30-cm MAR image plate area detector (MAR Research, Hamburg, Germany) with the wavelength tuned to  $\lambda$  = 1.0 Å. An in-house derivative data set was collected on a Mac Science DIP-2030H area detector equipped with a dual 30-cm image plate, with graphite monochromatized CuK $\alpha$  radiation ( $\lambda$  = 1.5418 Å) from a FR591 rotating anode generator with a double mirror x-ray focusing system (model MAC-XOS) as x-ray source (Enraf Nonius, Delft, The Netherlands). All data sets were collected at 100 K, integrated, and merged using the DENZO/SCALEPACK package (12) and software from the BIOMOL crystallographic package (Protein Crystallography Group, University of Groningen). Derivative data were scaled to the native data set using the program PHASES (13). Data-processing statistics are given in Table I.

**Structure Determination and Refinement**—The structure of the epoxide hydrolase from *A. radiobacter* AD1 was solved by the method of single isomorphous replacement supplemented by anomalous scattering, using both the in-house and synchrotron derivative data sets. A major heavy atom site (8.5  $\sigma$ ) for the ethyl mercury phosphate derivative was located in a difference Patterson map (12.0–4.5-Å data). The remaining 21 heavy atom positions were determined using difference Fourier techniques. Heavy atom position search, parameter refinement including anomalous data, and phase calculations were performed with PHASES (13) (Table I). The initial phases calculated at 3.7 Å yielded a figure of merit of 0.47 and were improved by solvent flattening and histogram matching techniques using the program DM (14). The non-crystallographic symmetry (NCS) operators (three orthogonal 2-fold axes) relating the 4 molecules in the asymmetric unit were determined with the help of FINDNCS,<sup>2</sup> using the 8 heavy atom sites with the highest occupancies. They were checked by comparing them with the rotation matrices calculated from a self-rotation function (16). An initial mask was built around one molecule in the asymmetric unit with the program MAMA (17); this mask was then used to refine the NCS operators by maximizing the correlation between the electron density maps of the 4 molecules in the asymmetric unit using the program IMP (17). Iterative cycles of density averaging, improvement of the mask, and refinement of the NCS operators, along with solvent flattening and phase extension to 2.6 Å resolution, resulted in a map of interpretable quality.

The model was traced using the program O (18). Nearly the complete polypeptide chain of one monomer could be interpreted in agreement with the amino acid sequence. By applying the refined NCS operators to the coordinates of the first molecule, coordinates for the other three molecules in the asymmetric unit were generated. The four molecules were then refined using the program X-PLOR (19). During the first runs of the refinement (simulated annealing and individual B-factor refinement), tight NCS restraints were applied (17), but in the final stage of the refinement (conventional positional refinement and individual B-factor refinement), they were gradually released or not even used at all for those residues that clearly showed different conformations in the 4 monomers in the asymmetric unit. The best refinement results were obtained using a flat bulk solvent correction. Special care was taken in the selection of the test set for the  $R_{\text{free}}$  calculation; the test set was selected by dividing the reflections in 102 thin-resolution shells to minimize the correlation between test set and working set reflections that could be caused by the presence of NCS (20). Water molecules were placed according to strict density and distance criteria, starting with the buried and NCS-related ones.

The final model consists of 4  $\times$  282 residues, 610 water molecules (33 of them refined with double positions), and 4 potassium ions. The crystallographic *R* factor and  $R_{\text{free}}$  are 19.0% and 22.7%, respectively. PROCHECK (21) and WHATCHECK (22) were used to assess the stereochemical quality. The structure was further analyzed using the

<sup>2</sup> G. Lu, <http://gamma.mbb.ki.se/~guoguang/findnscs.html>.

TABLE II

Refinement statistics and stereochemical quality of the final model

Resolution range (Å)	25–2.1
R factor <sup>a</sup> ( $R_{\text{free}}^b$ )	0.190 (0.227)
No. of residues in the asymmetric unit	4 × 282
No. of water molecules	610
No. of potassium ions	4
Average B-factor (Å <sup>2</sup> )	
Overall	28.3
Main chain	27.2
Side chain	28.7
Water molecules	33.5
Potassium ions	33.3
r.m.s. deviation from ideality	
bond lengths (Å)	0.008
bond angles (°)	1.338
Ramachandran plot	
Residues in most favored regions (%)	89.7
Residues in additional allowed regions (%)	9.3
Residues in generously allowed regions (%)	1.0

<sup>a</sup> R factor =  $\sum |F_{\text{obs}}| - |F_{\text{calc}}| / \sum |F_{\text{obs}}|$ , where  $F_{\text{obs}}$  and  $F_{\text{calc}}$  are the observed and calculated structure factor amplitudes, respectively.

<sup>b</sup> Free R-factor is calculated with 5% of the diffraction data selected randomly in 102 thin resolution shells that were not used during the refinement.

program VOIDOO (23), the programs from the CCP4 suite (14), the BIOMOL package, and the program DALI (24). Refinement statistics are given in Table II. The atomic coordinates and the structure factors have been deposited to the Protein Data Bank with the entry code 1ehy.

**Modeling of Asp<sup>246</sup>**—As a starting model, the atomic coordinates of the refined structure of the wild type epoxide hydrolase were used in which only the internal solvent molecules were retained. The crystal structure was energy-minimized prior to the modeling using a conjugate gradient routine implemented in X-PLOR (19). To completely remove the possible bias because of the conformation of the protein in the crystal, a slow-cooling molecular dynamics simulation (19) of 25 ps with temperature coupling (25) was performed in which the temperature was slowly reduced from 1000 K to 300 K. The missing loop 138–148 and the loop containing Asp<sup>246</sup> were built using the program O (18).

To model a likely conformation of the active Ephy enzyme, we assumed that the acid member of the catalytic triad, Asp<sup>246</sup>, should lie at interaction distance to the catalytic His<sup>275</sup> side chain, as found in many other members of the  $\alpha/\beta$  hydrolase-fold family (9). Haloalkane dehalogenase (PDB accession code 2HAD) (26) and bromoperoxidase A2 (PDB accession code 1BRO) (27) were used as templates to model the new Ephy Asp<sup>246</sup> position, analogous to Asp<sup>260</sup> of dehalogenase and Asp<sup>228</sup> of bromoperoxidase, respectively. Secondly, we assumed that the Gln<sup>134</sup> side chain should be removed from the active site, as it blocks the putative substrate binding site. This was done by giving the Pro<sup>132</sup>-Ile<sup>133</sup>-Gln<sup>134</sup> loop a similar conformation as the human pancreatic lipase (PDB accession code 1LPB) (28) Pro<sup>177</sup>-Ala<sup>178</sup>-Glu<sup>179</sup> motif, which has an equivalent topological position. The loop of residues 138–148, which is not observed in the electron density, was built like in the bromoperoxidase structure, connecting the core and the cap domains.

Several cycles of stereochemical regularization were performed using the REFI and LEGO option of O (18). The model was subsequently subjected to energy minimization to tidy up unacceptable close contacts and poor stereochemistry. To overcome the possibility that the energy-minimized structure was trapped in a local minimum, a second molecular dynamics-simulated annealing run was performed using the same setting as before. Extensive energy minimization was applied until convergence was reached, leading to a model with no residues outside the allowed regions in the Ramachandran plot (29) and good stereochemical quality (r.m.s. deviation bond lengths = 0.005 Å, r.m.s. deviation bond angles = 1.61°). Asp<sup>107</sup> and Asp<sup>131</sup> have slightly deviating backbone torsion angles, like in the x-ray structure.

Although the position of the modeled loop 132–148 is only one of the possible conformations it can assume, we are confident that the rebuilding of the loop containing Asp<sup>246</sup>, in a fashion common to many  $\alpha/\beta$  hydrolase-fold enzymes, gives a plausible picture of the catalytic site of the fully active epoxide hydrolase.



FIG. 1. Schematic view of the secondary structure elements (from DSSP (38)) of the epoxide hydrolase monomer. Ribbon representation drawn using MOLSCRIPT (39) is shown;  $\alpha$ -helices,  $\beta$ -strands, and coils are represented by helical ribbons, arrows, and ropes, respectively. The  $\alpha$ -helices of the cap domain are shown in dark gray.

## RESULTS

**Quality of the Model**—Epoxide hydrolase from *A. radiobacter* AD1 (Ephy) crystallizes in the monoclinic space group C2, with 4 molecules in the asymmetric unit. A superimposition of the C $\alpha$  atoms of the four molecules gave an average r.m.s. difference of 0.24 Å for molecules B, C, and D and a higher r.m.s. difference of 0.40 Å if molecule A is included. All results discussed below apply to all 4 molecules (A, B, C, and D) unless stated otherwise. The final model consists of 4 × 282 residues, 610 water molecules (33 of them refined with double positions), and 4 potassium ions, originating from the crystallization buffer, one for each molecule in the asymmetric unit. In each monomer (294 residues), the first N-terminal residue (Met) is not visible nor is there interpretable electron density for the loop 138–148. The final crystallographic R factor and  $R_{\text{free}}$  values are 19.0% and 22.7%, respectively. The r.m.s. deviations from ideal geometry are 0.008 Å for bond lengths and 1.338° for bond angles. No residues are in the disallowed regions of the Ramachandran plot (29). Pro<sup>39</sup> was found in a *cis* conformation.

**Overall Structure**—The Ephy monomer has a nearly globular shape with approximate dimensions of 48 × 47 × 47 Å<sup>3</sup>. It consists of two domains: domain I (or “core” domain), which shows the typical features of the  $\alpha/\beta$  hydrolase-fold topology (9), and the mainly  $\alpha$ -helical domain II (or “cap” domain), which lies on top of domain I (Figs. 1 and 2). The core domain comprises amino acids 1–137 and 219–294, and it consists of a central eight-stranded  $\beta$ -sheet with seven parallel strands (only the second strand is antiparallel). The  $\beta$ -sheet is flanked on both sides by  $\alpha$ -helices, two on one side and four on the other. Helix  $\alpha$ 9 is a one-turn  $3_{10}$  helix. Domain II, containing  $\alpha$ -helices  $\alpha$ 4 to  $\alpha$ 8, forms a large excursion between  $\beta$ -strands  $\beta$ 6 and  $\beta$ 7 of the core domain. It has a double-layered structure with helices  $\alpha$ 7 and  $\alpha$ 8 located between the core domain and the plane formed by  $\alpha$ 4,  $\alpha$ 5, and  $\alpha$ 6.

**Active Site**—The proposed active-site residues (6) Asp<sup>107</sup> and His<sup>275</sup> are located in a predominantly hydrophobic internal cavity between domains I and II. The core domain contributes to the lining of the cavity with residues Gly<sup>37</sup>, Trp<sup>38</sup>, Pro<sup>39</sup>,



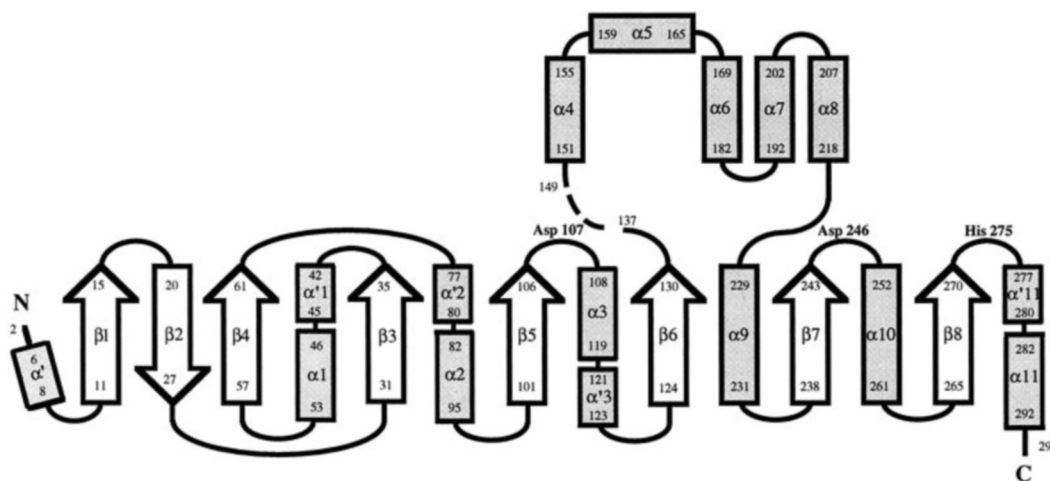


FIG. 2. Secondary structure topology diagram and location of the catalytic triad residues, Asp<sup>107</sup>, Asp<sup>246</sup>, and His<sup>275</sup>. The dashed line represents the missing loop 138–148. Short  $3_{10}$  helices are located at the N terminus ( $\alpha'$ ), between  $\beta 3$  and  $\alpha 1$  ( $\alpha'1$ ), between  $\beta 4$  and  $\alpha 2$  ( $\alpha'2$ ), and between  $\alpha 3$  and  $\beta 6$  ( $\alpha'3$ ). The last  $\alpha$ -helix shows a conspicuous bend at residue 281 ( $\alpha'11$ - $\alpha 11$ ) because of the presence of Pro<sup>282</sup> in the center of the helix.

Glu<sup>44</sup>, His<sup>106</sup>, Asp<sup>107</sup>, Phe<sup>108</sup>, Ile<sup>133</sup>, Phe<sup>137</sup>, Ile<sup>219</sup>, His<sup>275</sup>, Phe<sup>276</sup>, Val<sup>279</sup>. The cap domain supplies Tyr<sup>152</sup>, Trp<sup>183</sup>, and Tyr<sup>215</sup> (Fig. 3).

Asp<sup>107</sup> is situated at the very sharp “nucleophile elbow” between the central strand  $\beta 5$  and helix  $\alpha 3$ . At this topological position, all  $\alpha/\beta$  hydrolase-fold enzymes present the nucleophile, which can either be Ser, Cys, or Asp (9). The ( $\phi$ ,  $\psi$ ) angles of Asp<sup>107</sup> are slightly unfavorable ( $\phi = 57^\circ$ ,  $\psi = -124^\circ$ ), but its conformation is stabilized by a network of hydrogen bonds involving residues of the sharp turn, as has been found in other  $\alpha/\beta$  hydrolase enzymes (9). In addition, the main chain nitrogen atom of Asp<sup>107</sup> interacts via a hydrogen bond with the backbone oxygen atom of Asp<sup>131</sup>, the other residue with slightly deviating backbone torsion angles ( $\phi = 31^\circ$ ,  $\psi = 69^\circ$ ). Furthermore, the side chain of Asp<sup>107</sup> is stabilized by a hydrogen bond of its O $\delta 2$  atom with the backbone amide groups of Trp<sup>38</sup> and Phe<sup>108</sup> and by a salt bridge between the O $\delta 1$  atom of Asp<sup>107</sup> and the Ne2 atom of the His<sup>275</sup> side chain.

An  $\sim 20$ -Å long tunnel, filled with water molecules, is located between  $\alpha$ -helices  $\alpha 1$ ,  $\alpha 10$ , the loop connecting  $\alpha$ -helix  $\alpha 1$  and  $\beta$ -strand  $\beta 3$  of the core domain, and  $\alpha 7$  of the cap domain (Fig. 4). This tunnel leads to the back of the active-site cavity, and it is perfectly suited to replenish the hydrolytic water molecule at hydrogen bond distance to the Ne2 atom of the His<sup>275</sup> side chain (Fig. 3) after the reaction. In our structure, the active site cavity is exposed to the solvent from the front part too, where the missing loop is located. Because of the position of the hydrolytic water molecule in the back of the active site, it is likely that the substrate enters the active-site cavity from the front part.

Asp<sup>246</sup> has been proposed to be the acidic member of the catalytic triad, responsible for assisting His<sup>275</sup> in activating the water molecule that hydrolyzes the ester intermediate formed at Asp<sup>107</sup> (6). Asp<sup>246</sup> is located in a turn between strand  $\beta 7$  and helix  $\alpha 10$ , in a position topologically conserved within the  $\alpha/\beta$  hydrolase-fold family (Fig. 2) (9). However, in our crystal structure Asp<sup>246</sup> is not at interacting distance from His<sup>275</sup>. Instead the loop containing this residue is pulled away from the active site, and the Asp<sup>246</sup> side chain is pointing into the solvent. This is probably the result of crystal packing forces because helix  $\alpha 10$  of molecule A, which follows the loop containing Asp<sup>246</sup>, is involved in an intermolecular contact with helix  $\alpha 10$  of molecule B. A similar contact exists between molecules C and D, which even involves an intermolecular disulfide bridge be-

tween Cys(C)<sup>248</sup> and Cys(D)<sup>248</sup>. The absence of this disulfide bond between molecules A and B results in a slightly different conformation of the loop containing Cys<sup>248</sup> in molecule A compared with the other three molecules in the asymmetric unit. As a consequence, the difference between the C $\alpha$  positions of molecules A, B, C, and D (average r.m.s. difference of 0.40 Å) is higher than for the B, C, and D molecules only (r.m.s. difference of 0.24 Å). The conformational plasticity of the region between residues 244 and 257 is also reflected by very high B-factors (between 28 Å<sup>2</sup> and 84 Å<sup>2</sup>) and a not easily interpretable electron density map, often poorly defined or showing multiple conformations even for the backbone. The space vacated by Asp<sup>246</sup> makes it possible for the side chain of Gln<sup>134</sup> to move into the active site, occupying the site where the substrate is likely to be bound (Fig. 3). Its position is stabilized by a hydrogen bonding network involving the hydroxyl groups of Tyr<sup>152</sup> and Tyr<sup>215</sup> and the carboxyl oxygen O $\delta 1$  of Asp<sup>107</sup>.

**Comparison with  $\alpha/\beta$  Hydrolases**—The folding of Ephy strongly resembles that of bromoperoxidase A2 from *Streptomyces aureofaciens* (27) (BpA2, PDB accession code 1BRO; r.m.s. deviation  $\sim 1.7$  Å for 193 C $\alpha$  atoms) and haloalkane dehalogenase from *Xanthobacter autotrophicus* (10, 26, 30) (Dh1A, PDB accession code 2HAD; r.m.s. deviation  $\sim 2.0$  Å for 204 C $\alpha$  atoms) and a number of other members of the  $\alpha/\beta$  hydrolase-fold family (9). The matching is best for the central  $\beta$ -sheet and for helices  $\alpha 2$  and  $\alpha 3$  (Fig. 5), but all other structural elements are equivalent as well, especially in the regions close to the catalytic residues. The  $\alpha$ -helices in the cap domain superimpose less well, showing a different relative orientation. These helices contribute several residues important for the interaction with substrates.

Despite a low sequence homology (33% homology, 20% identity), the structural similarity of epoxide hydrolase and haloalkane dehalogenase is particularly interesting. These enzymes have both an Asp-His-Asp catalytic triad. Asp<sup>107</sup> and His<sup>275</sup> of Ephy superimpose very well on Asp<sup>124</sup> and His<sup>289</sup> of Dh1A; their side chains are in the same relative position and make similar hydrogen bonds. In dehalogenase the halogen atom of the substrate is bound between the indole ring N-atoms of Trp<sup>125</sup> and Trp<sup>175</sup>. In epoxide hydrolase, Phe<sup>108</sup> and Trp<sup>183</sup> occupy the equivalent positions, suggesting that they may be involved in substrate binding (6). However, a stabilizing structural role for Phe<sup>108</sup> is also conceivable, as it has a “T-shaped” interaction with the Tyr<sup>215</sup> side chain (31). In dehalogenase,

FIG. 3. Stereo view of residues lining the active site of epoxide hydrolase. Residues and water molecules are drawn in ball and stick representation using MOLSCRIPT (39). The catalytic water molecule is labeled WAT.

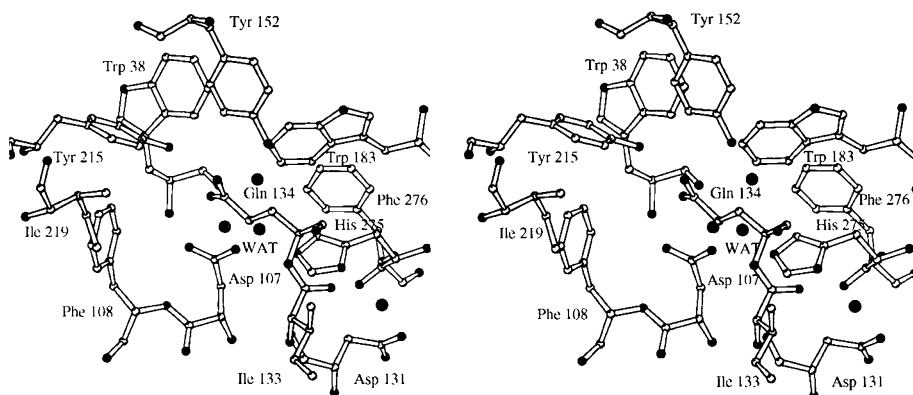


FIG. 4. Stereo view of the tunnel connecting the back of the active site with the protein surface. The tunnel was calculated with VOIDOO (23) using a probe with radius 1.2 Å. The core and the cap domain are shown in light and dark gray, respectively. Side chains of Asp<sup>107</sup> and His<sup>275</sup> are in ball and stick representation. The figure was drawn using BOBSCRIPT (15).

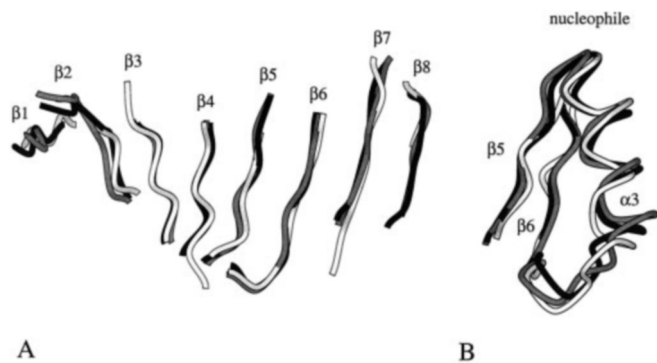
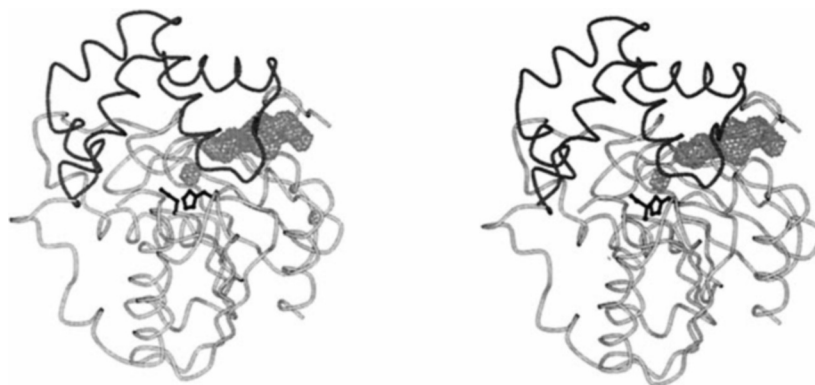


FIG. 5. Superimposition of the cores of epoxide hydrolase from *A. radiobacter* AD1 (black), haloalkane dehalogenase from *X. autotrophicus* (white), and bromoperoxidase A2 from *S. aureofaciens* (gray). A, superimposition of the central  $\beta$ -sheet. B, superimposition of the region around the position of the nucleophile, with  $\beta$ -strand 5,  $\alpha$ -helix 3, and  $\beta$ -strand 6. The figure was produced using MOLSCRIPT (39).

the O $\delta$ 2 atom of Asp<sup>124</sup>, which in the putative transition state will become negatively charged, is stabilized by interaction with the main chain nitrogen atoms of residues 125 and 56. Asp<sup>107</sup> O $\delta$ 2 in Ephy has similar interactions with the amide nitrogen atoms of residues 108 and 38, suggesting Phe<sup>108</sup> and Trp<sup>38</sup> as part of the oxyanion hole.

**Modeling of Asp<sup>246</sup>**—As mentioned above, the third catalytic residue, Asp<sup>246</sup>, is pulled out of the active site. However, the positions of Asp<sup>260</sup> in haloalkane dehalogenase and Asp<sup>228</sup> in bromoperoxidase A2 give a reliable suggestion where Asp<sup>246</sup> should be located in the active conformation of Ephy. Superposition of the  $\beta$ -sheets of Dh1A and BpA2 on that of Ephy brings the O $\delta$ 2 atom of Asp<sup>260</sup> of dehalogenase and Asp<sup>228</sup> of bromoperoxidase in coincidence with the water molecule in Ephy, which is hydrogen-bonded to N $\delta$ 1 of His<sup>275</sup> and O $\delta$ 2 of Asp<sup>131</sup> (Fig. 6). This information was used to model a likely conformation of the “active” Ephy enzyme, with Dh1A, BpA2, and human

pancreatic lipase (Hpl) structures as templates for reconstructing the Ephy loops containing Asp<sup>246</sup> and Gln<sup>134</sup> (See “Experimental Procedures”).

The final model shows an intact and empty active site cavity, capable of accommodating substrates. It is lined with Gly<sup>37</sup>, Trp<sup>38</sup>, Pro<sup>39</sup>, Glu<sup>44</sup>, His<sup>106</sup>, Asp<sup>107</sup>, Phe<sup>108</sup>, Ile<sup>133</sup>, Phe<sup>137</sup>, Tyr<sup>152</sup>, Trp<sup>183</sup>, Tyr<sup>215</sup>, Ile<sup>219</sup>, Cys<sup>248</sup>, His<sup>275</sup>, Phe<sup>276</sup>, and Val<sup>279</sup> (Fig. 7). Asp<sup>246</sup> is hydrogen-bonded to the His<sup>275</sup> N $\delta$ 1, and it now occupies the position where the acidic member of the catalytic triad is normally found in  $\alpha/\beta$  hydrolase-fold enzymes. The rest of the active site has undergone only minor changes in the relative positions of the atoms. The hydrolytic water molecule is still present at hydrogen bond distance to the His<sup>275</sup> Ne2 atom. The Tyr<sup>152</sup> and Tyr<sup>215</sup> hydroxyl groups, which in the crystal structure were hydrogen-bonded to the Gln<sup>134</sup> side chain, still point in the same direction, enabling them to donate the proton needed for opening of the epoxide ring (Fig. 8).

## DISCUSSION

**Active Site and Substrate Binding**—Epoxide hydrolase has a two-domain structure (Fig. 1). The core domain displays an  $\alpha/\beta$  hydrolase-fold topology, which provides the scaffolding for the catalytic triad residues Asp<sup>107</sup>, His<sup>275</sup>, and Asp<sup>246</sup>, whereas the  $\alpha$ -helical cap domain contributes several residues important for the interaction with substrates. The active site is located in a cavity between the two domains, which contains Asp<sup>107</sup> and His<sup>275</sup>. Asp<sup>107</sup> is the nucleophile that attacks the substrate carbon atom in the first step of the reaction, whereas His<sup>275</sup> activates the water molecule that hydrolyzes the ester intermediate in the second reaction step (6). Indeed, in the crystal structure, a water molecule is visible at hydrogen bond distance to the Ne2 atom of the His<sup>275</sup> side chain. Because of the crystallization pH (7.0), in the x-ray structure, His<sup>275</sup> is stabilized by a salt bridge with Asp<sup>107</sup> O $\delta$ 1. At the optimum pH for catalysis (8.4–9.0) His<sup>275</sup> Ne2 is most likely deprotonated and therefore able to activate the water molecule located nearby. In

FIG. 6. Stereo view of the water-mediated interaction between Asp<sup>131</sup> and His<sup>275</sup> and of the oxyanion hole in epoxide hydrolase. Hydrogen bonds are shown as dashed lines. Side chains, water molecules, and the HGWP motif are in ball and stick representation. The catalytic water molecule is labeled WAT. The figure was produced using MOLSCRIPT (39).

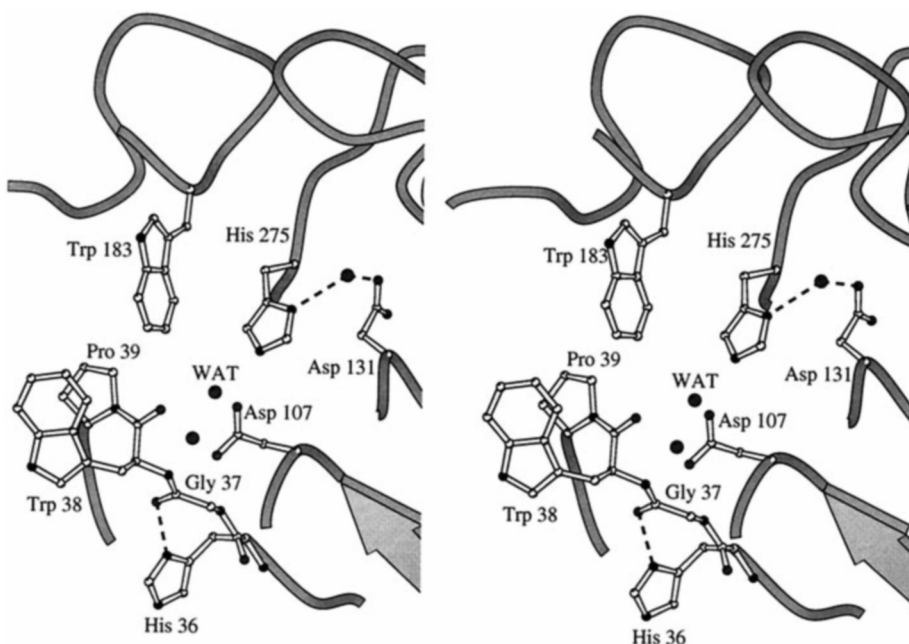
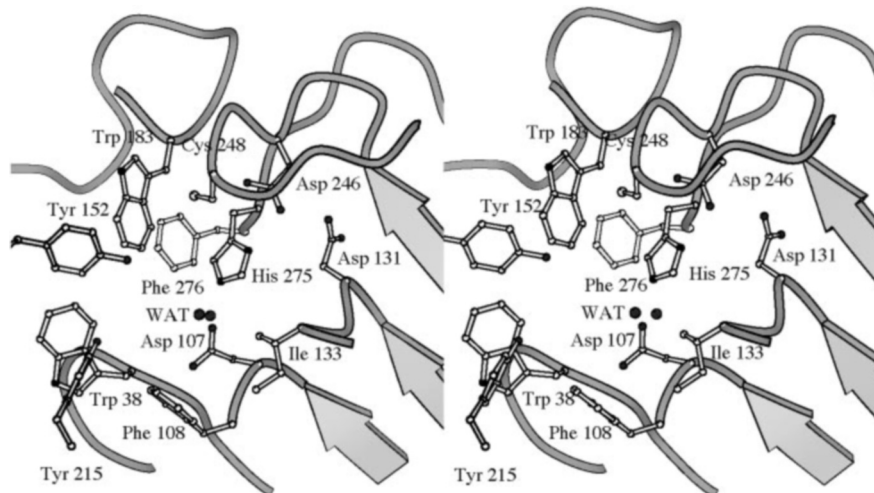


FIG. 7. Stereo view of the active site of the model of epoxide hydrolase. Side chains and water molecules are in ball and stick representation. The catalytic water molecule is labeled WAT. The figure was drawn using MOLSCRIPT (39).



the crystal structure, this water molecule is in contact with the solvent via a narrow tunnel between the core and cap domains (Fig. 4). This tunnel resembles the active site back entrance in bromoperoxidase A2, which was proposed to provide access to the active site for small molecules participating in the reaction, like peroxide and halide, or to expel water molecules from the active site during substrate binding (27). In epoxide hydrolase, it seems more likely that the tunnel serves to replenish the hydrolytic water molecule after the reaction has been completed.

The third member of the catalytic triad, Asp<sup>246</sup>, assists His<sup>275</sup> in activating the hydrolytic water molecule (6). To our surprise it is not at hydrogen bonding distance from the Nδ1 atom of His<sup>275</sup>, but it has moved away into the solvent region. This is most probably a consequence of crystal packing forces: the Asp<sup>246</sup> → Ala mutation strongly decreases the activity of the enzyme (~0.5% of the wild type activity) (6), and such a dramatic effect on activity is difficult to rationalize for the position of the residue as observed in our crystals. The exposed position of Asp<sup>246</sup> has made it possible for the Gln<sup>134</sup> side chain to move into the active site and block it (Fig. 3). Because a Gln<sup>134</sup> → Ala mutant has an activity comparable with that of wild-type enzyme, it is unlikely that Gln<sup>134</sup> is normally present

in the active site. However, human microsomal epoxide hydrolase has been reported to be inhibited by amides (32). The *A. radiobacter* epoxide hydrolase shows competitive inhibition by amides as well, especially by compounds like phenylacetamide ( $K_i = 30 \mu\text{M}$ ).<sup>3</sup> Therefore, we conclude that the Gln<sup>134</sup> side chain may act as such an inhibitor, mimicking the binding mode of epoxide substrates. Thus, the combination of crystal contacts of helix  $\alpha 10$  (residues 252 to 261) and the affinity of the active site for amide compounds have probably led to the observed exposed position of Asp<sup>246</sup>. Nevertheless, the high structural similarity (Fig. 5) between the core domains of epoxide hydrolase, haloalkane dehalogenase, bromoperoxidase A2, and human pancreatic lipase allowed us to use the latter three enzyme structures as templates to remodel the loops containing Asp<sup>246</sup> and Gln<sup>134</sup>. The result is a plausible model of the active site in the fully active enzyme (Fig. 7).

In the crystal structure the Gln<sup>134</sup> side chain oxygen is hydrogen-bonded to the hydroxyl group of Tyr<sup>152</sup> and Tyr<sup>215</sup> (Fig. 3). These two tyrosines are the only acidic functional groups present in the active site that can facilitate the opening

<sup>3</sup> R. Rink and D. B. Janssen, manuscript in preparation.



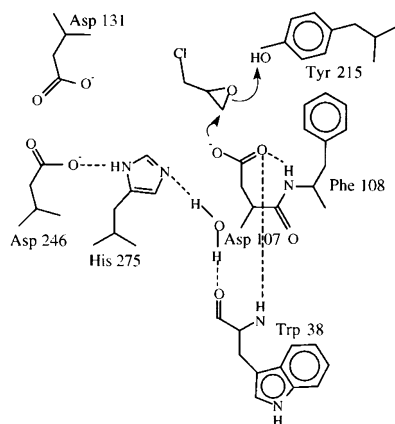


FIG. 8. **Schematic representation of the catalytic mechanism of epoxide hydrolase.** The Michaelis complex with epichlorohydrin is shown before the formation of covalent intermediate, which is indicated by arrows. Hydrogen bonds are shown as dashed lines.

of the epoxide ring by hydrogen bonding and protonating the epoxide oxygen. In agreement with this hypothesis, mutagenesis studies of these tyrosines have shown that only a double Tyr<sup>152</sup> and Tyr<sup>215</sup> are able to provide the proton needed for the opening of the epoxide ring.<sup>4</sup> Because Tyr<sup>215</sup> is absolutely conserved within the epoxide hydrolase family and Tyr<sup>152</sup> is mostly conserved in the soluble epoxide hydrolases, it is likely that the Tyr activation is a general property of this class of enzymes (Fig. 8). In the past, one of three lysines, Lys<sup>173</sup>, Lys<sup>174</sup>, and Lys<sup>177</sup>, was proposed to be involved in the protonation (6), but the crystal structure of Ephy unambiguously shows that these three lysine residues are located far from the active site, exposed to the solvent on top of the cap domain.

**Position and Function of Asp<sup>131</sup>.**—The Asp<sup>246</sup> → Ala mutation resulted in a strong reduction of enzymatic activity. Nevertheless, this mutant still has some residual activity (~0.5% that of wild type activity), indicating the importance of Asp<sup>246</sup> in catalysis but not its essentiality (6). The three-dimensional structure of Ephy shows the presence of another aspartic acid, Asp<sup>131</sup>, which may act as a backup of Asp<sup>246</sup> (Fig. 3). Asp<sup>131</sup> is located between strand  $\beta$ 6 and the first helix of the cap domain, with its side chain in close contact with the imidazole ring of the catalytic His<sup>275</sup>. A water molecule, present in all four monomers in the asymmetric unit, bridges the interaction between O $\delta$ 2 of Asp<sup>131</sup> and N $\delta$ 1 of His<sup>275</sup> (Fig. 6).

Asp<sup>131</sup> is at an equivalent position to Asn<sup>148</sup> in haloalkane dehalogenase. In the dehalogenase, Asn<sup>148</sup> is involved in a hydrogen-bonding stabilization of the active site (10, 26, 30). Like Asn<sup>148</sup>, Asp<sup>131</sup> in Ephy also shows slightly unusual backbone torsion angles. Furthermore, in the dehalogenase, the activity of an Asp<sup>260</sup> → Asn mutant could be restored by an Asn<sup>148</sup> → Asp/Glu mutation. This shows that the catalytic triad in Dhla can be either Asp-His-Asp<sup>260</sup> or Asp-His-Asp<sup>148</sup> (33). The same could be true for Ephy, where Asp<sup>131</sup> could take over the function of Asp<sup>246</sup> by a simple rotation around the  $\chi$ 1 and  $\chi$ 2 torsion angles, which would allow its side chain to be hydrogen-bonded to His<sup>275</sup> N $\delta$ 1.

A similar shift of functional residues has been observed for *Pseudomonas glumae* lipase (Pgl) (34) and Hpl (35), two other members of the  $\alpha/\beta$  hydrolase-fold family. In Pgl, Glu<sup>288</sup> can take over the role of Asp<sup>263</sup> as the acid residue of the catalytic triad. Glu<sup>288</sup> O $\epsilon$ 2 and Asp<sup>263</sup> O $\delta$ 2 of Pgl match the positions of

Asp<sup>131</sup> O $\delta$ 2 and of its hydrogen-bonded water molecule in Ephy. In human pancreatic lipase, an alternative catalytic triad is present in which the acid catalytic residue is shifted from  $\beta$ -strand 7 to  $\beta$ -strand 6 at position 176. Asp<sup>176</sup> of Hpl overlaps with Asp<sup>131</sup> in Ephy, with the Asp<sup>176</sup> O $\delta$ 2 atom matching the position of the water molecule hydrogen-bonded to Asp<sup>131</sup> in Ephy. These observations make Asp<sup>131</sup> a very interesting residue for site-specific mutational studies to further probe its role in catalysis.

**Oxyanion Hole.**—A conserved HGXP tetrapeptide motif (X = any amino acid) is found in epoxide hydrolases and other  $\alpha/\beta$  hydrolase-fold enzymes (2, 3). The HGWP motif of Ephy is located in a sharp *cis*-proline turn (Trp<sup>38</sup>-Pro<sup>39</sup>), which is stabilized by the hydrogen bond between His<sup>36</sup> N $\delta$ 1 and the backbone carbonyl oxygen of Gly<sup>37</sup> (Fig. 6).

In haloalkane dehalogenase, this sequence motif is HGEP, and the main chain N atom of the glutamate residue (Glu<sup>56</sup>) is, together with the peptide nitrogen atom of residue Trp<sup>125</sup>, part of the oxyanion hole, interacting with the O $\delta$ 2 atom of the nucleophile Asp<sup>124</sup> (10, 26). In epoxide hydrolase, a similar hydrogen bonding pattern is present between the O $\delta$ 2 atom of the nucleophile Asp<sup>107</sup> and the amide nitrogen atoms of Trp<sup>38</sup> and Phe<sup>108</sup>. Thus these peptide nitrogen atoms are in an optimal position to stabilize the negative charge that develops on the O $\delta$ 2 atom of the nucleophile during the hydrolysis of the ester intermediate. In addition, the negative charge on Asp<sup>107</sup> O $\delta$ 2 may be further stabilized by the  $\alpha$ -helix dipole of helix  $\alpha$ 3 (36).

A second role of the tetrapeptide motif may be in stabilizing the position of the putative hydrolytic water molecule (Fig. 6). Indeed, in the crystal structure this water molecule is at interacting distance to the backbone oxygen atom of Trp<sup>38</sup>.

These essential structural functions may explain the importance of the HGXP motif for enzymatic activity within the epoxide hydrolase family, as already demonstrated by mutation of His to Ala in the rat microsomal epoxide hydrolase (37).

**Conclusions.**—The x-ray structure reveals for the first time the fold of an epoxide hydrolase and provides novel, detailed information on the residues involved in the enzymatic mechanism. It localizes the catalytic residues, the hydrolytic water molecule, and the position of the oxyanion hole, and it proposes a possible backup for the acidic member of the catalytic triad. Most importantly, it unambiguously identifies the previously unanticipated Tyr<sup>152</sup>/Tyr<sup>215</sup> as the acidic group responsible for binding and possibly protonation of the transition state of the formation of the ester intermediate. The residues important for catalysis are conserved within the epoxide hydrolase family. Therefore all these structural features are likely to be shared by other epoxide hydrolases and allow us to gain a better understanding of the behavior and mechanism of this class of biologically and biotechnologically important enzymes. At present we are investigating the structural basis of the enzymatic enantioselectivity by mutation analysis and by docking the substrates in the modeled active site.

**Acknowledgment.**—We thank A. Savoia and the staff of the x-ray diffraction beamline at the ELETTRA synchrotron, Trieste (I), for the synchrotron data collection facilities and assistance.

#### REFERENCES

1. Archelas, A., and Furstoss, R. (1998) *Trends Biotechnol.* **16**, 108–116
2. Lacourciere, G. M., and Armstrong, R. N. (1994) *Chem. Res. Toxicol.* **7**, 121–124
3. Arand, M., Grant, D. F., Beetham, J. K., Friedberg, T., Oesch, F., and Hammock, B. D. (1994) *FEBS Lett.* **338**, 251–256
4. Hernandez, O., and Bend, J. R. (1982) *Metabolic Basis of Detoxication*, pp. 207–228, Academic Press, Inc., New York
5. Jacobs, M. H. J., van den Wijngaard, A. J., Pentenga, M., and Janssen, D. B. (1991) *Eur. J. Biochem.* **202**, 1217–1222
6. Rink, R., Fennema, M., Smids, M., Dehmelt, U., and Janssen, D. B. (1997) *J. Biol. Chem.* **272**, 14650–14657
7. Misawa, E., Chion, C. K. C. K., Archer, I. V., Woodland, M. P., Zhou, N. Y.,

<sup>4</sup> R. Rink, J. H. Lutje Spelberg, R. J. Pieters, J. Kingma, M. Nardini, R. M. Kellogg, B. W. Dijkstra, and D. B. Janssen, manuscript in preparation.

- Carter, S. F., Widdowson, D. A., and Leak, D. J. (1998) *Eur. J. Biochem.* **253**, 173–183
8. Lutje Spelberg, J. H., Rink, R., Kellogg, R. M., and Janssen, D. B. (1998) *Tetrahedron: Asymmetry* **9**, 459–466
9. Ollis, D. L., Cheah, E., Cygler, M., Dijkstra, B., Frolow, F., Franken, S. M., Harel, M., Remington, S. J., Silman, I., Schrag, J., Sussman, J. L., Verschuere, K. H. G., and Goldman, A. (1992) *Protein Eng.* **5**, 197–211
10. Verschuere, K. H. G., Seljée, F., Rozeboom, H. J., Kalk, K. H., and Dijkstra, B. W. (1993) *Nature* **363**, 693–698
11. Jancarik, J., and Kim, S. H. (1991) *J. Appl. Crystallogr.* **24**, 409–411
12. Otwinowski, Z., and Minor, W. (1997) *Methods Enzymol.* **276**, 307–326
13. Furey, W., and Swaminathan, S. (1997) *Methods Enzymol.* **277**, 590–620
14. Collaborative Computational Project Number 4 (1994) *Acta Crystallogr. Sec. D* **50**, 760–763
15. Esnouf, R. M. (1997) *J. Mol. Graphics* **15**, 132–134
16. Navaza, J., and Saludjian, P. (1997) *Methods Enzymol.* **276**, 581–594
17. Kleywegt, G. J., and Jones, T. A. (1996) *Acta Crystallogr. Sec. D* **52**, 842–857
18. Jones, T. A., Zou, J. Y., Cowan, S. W., and Kjeldgaard, M. (1991) *Acta Crystallogr. Sec. A* **47**, 110–119
19. Brünger, A. T. (1992) *X-PLOR: A System for X-ray Crystallography and NMR*, Version 3.1, Yale University Press, New Haven, Connecticut
20. Kleywegt, G. J., and Jones, T. A. (1995) *Structure (Lond.)* **15**, 535–540
21. Laskowski, R. A., MacArthur, M. W., Moss, D. S., and Thornton, J. M. (1993) *J. Appl. Crystallogr.* **26**, 283–291
22. Hooft, R. W. W., Vriend, G., Sander, C., and Abola, E. E. (1996) *Nature* **381**, 272
23. Kleywegt, G. J., and Jones, T. A. (1994) *Acta Crystallogr. Sec. D* **50**, 178–185
24. Holm, L., and Sander, C. (1994) *Proteins* **3**, 165–173
25. Berendsen, H. J. C., Postma, J. P. M., van Gunsteren, W. F., Di Nola, A., and Haak, J. R. (1984) *J. Chem. Phys.* **81**, 3684–3690
26. Verschuere, K. H. G., Franken, S. M., Rozeboom, H. J., Kalk, K. H., and Dijkstra, B. W. (1993) *J. Mol. Biol.* **232**, 856–872
27. Hecht, H. J., Sobek, H., Haag, T., Pfeifer, O., and van Pée, K.-H. (1994) *Nat. Struct. Biol.* **1**, 532–537
28. Egloff, M. P., Marguet, F., Buono, G., Verger, R., Cambillau, C., and van Tilbeurgh, H. (1995) *Biochemistry* **34**, 2751–2762
29. Ramakrishnan, C., and Ramachandran, G. N. (1965) *J. Mol. Biol.* **7**, 95–99
30. Franken, S. M., Rozeboom, H. J., Kalk, K. H., and Dijkstra, B. W. (1991) *EMBO J.* **10**, 1297–1302
31. McGaughey, G. B., Gagné, M., and Rappé, A. K. (1998) *J. Biol. Chem.* **273**, 15458–15463
32. Kerr, B. M., and Levy, R. H. (1990) *Drug Metab. Dispos.* **18**, 540–542
33. Krooshof, G. H., Kwant, E. M., Damborsky, J., Koca, J., and Janssen, D. B. (1997) *Biochemistry* **36**, 9571–9580
34. Noble, M. E. M., Cleasby, A., Johnson, L. N., Egmond, M. R., and Frenken, L. G. J. (1993) *FEBS Lett.* **331**, 123–128
35. Winkler, F. K., D'Arcy, A., and Hunziker, W. (1990) *Nature* **343**, 771–774
36. Hol, W. G. J., van Duijnen, P. T., and Berendsen, H. J. C. (1978) *Nature* **273**, 443–446
37. Bell, P. A., and Kasper, C. B. (1993) *J. Biol. Chem.* **268**, 14011–14017
38. Kabsch, W., and Sander, C. (1983) *Biopolymers* **22**, 2577–2637
39. Kraulis, P. (1991) *J. Appl. Crystallogr.* **24**, 946–950